Multi-Platform Target Detection using Multi-Channel Coherence Analysis and Robustness to the Effects of Disparity

Nick Klausner*, J. Derek Tucker*†, and Mahmood R. Azimi-Sadjadi*
*Department of Electrical and Computer Engineering
Colorado State University, Fort Collins, Colorado 80523-1373
Email: {nklausne,dtucker,azimi}@engr.colostate.edu
†Naval Surface Warfare Center - Panama City Division
Panama City, FL 32407-7001
Email: james.d.tucker@navy.mil

***Abstract*—The use of multiple disparate platforms in many remote sensing and surveillance applications allows one to exploit the coherent information shared among all sensory systems thereby potentially reducing the risk of making single-sensory biased detection and classification decisions. This paper introduces a target detection method based upon multi-channel coherence analysis (MCA) framework which optimally decomposes the multi-channel data to analyze their linear dependence or coherence. This decomposition then allows one to extract MCA features that can be used to implement a coherence-based detector. This detector is applied to a data set of simulated disparate sonar imagery provided by the Naval Surface Warfare Center (NSWC) - Panama City. This database contains images of both targets and non-targets with various variabilities with respect to resolution, signal-to-noise ratio (SNR), target and non-target types, etc. Sensitivity analyses are then carried out in order to gauge the performance under such variablities that may be encountered in disparate multi-platform detection problems. Performance of the detection method will be given in terms of probability of detection (P_d), probability of false alarm (P_{fa}), and the receiver operating characteristic (ROC) curves.**

***Index Terms*—Binary hypothesis testing, disparate sonar platforms, multi-channel coherence analysis, underwater target detection**

I. Introduction

The problem of developing a robust underwater target detection and classification system that can operate with multiple disparate sensing systems poses many technical challenges and has recently attracted considerable interest in many areas of remote sensing. In the traditional centralized processing scheme preliminary detection, feature extraction, and object classification are performed based upon the data collected by every individual sensor platform. Final decision making usually takes place at the fusion center using some type of decision-level, feature-level, or combined fusion mechanism. However, decision-making based upon individual sensory data can lead to incomplete, degraded, or locally biased (sensor-level) decisions resulting in a poor final detection and classification performance at the fusion center. Thus, new methods are needed to detect, isolate, and represent, in terms of some pertinent attributes, the *coherent* or common information shared among the multiple data sets. This can be an extremely challenging problem due to the disparate nature of the problem and variations in the operating conditions which can often arise in many multi-platform sensory systems.

An approach to multiple-channel signal detection was considered in [1] by introducing the Generalized Coherence (GC) estimate, a nonparametric measure of the information shared by any number of channels. This measure is formed by finding the determinant of the Gram matrix formed by all N channels normalized by the product of the squared norm of each channel. This GC measure exhibits many attractive properties including invariance to constant channel gain. The GC measure is shown to have an appealing geometrical interpretation as it is noted that the determinant of the Gram matrix heuristically measures the squared volume of a parallelepiped in n-D space, where n corresponds to the dimension of each channel. Thus, the more the channels have in common, the smaller the normalized volume, and the closer the GC estimate to one. The distribution of the GC estimate is then derived under conditions of white Gaussian noise, theoretically allowing one to determine thresholds corresponding to a particular false alarm rate. Simulations are then provided demonstrating the GC estimate's capability in multiple-channel detection problems. The existing work [2] - [3] in the area of target detection from sonar imagery has primarily been focused on one sonar platform, with fusion across multiple algorithms. In [4], the adaptive clutter filter detector in [3] is individually applied to three different sonar images varying in frequency and bandwidth. Final classification is done using an optimal set of features using a nonlinear log-likelihood ratio test where the decisions of the individual detector and classifier are fused. The optimal set of features is determined based upon cascading another classifier on the previous classifier during the training stage. This is done as a repeated application during the training stage where at each iteration the threshold and optimal feature set is chosen and updated. In our previous work [5], we developed a new framework for multi-sensor

coherence analysis using Multi-Channel Coherence Analysis (MCA) [6] that can be applied to the data collected using multiple disparate sonar systems. Using this method allows for the simultaneous detection and feature extraction of coherent target information among multiple disparate sonar images.

This paper reviews the N-channel coherence-based detector using the MCA framework [5]. This detector exploits the coherence of objects present in N disparate channels based on the assumption that the presence of objects in all data sets will lead to a higher level of coherence compared to that of noise alone. New expressions for the log-likelihood ratio and J-divergence in the MCA framework are provided and used for the simultaneous detection of targets from N disparate sonar data. In order to examine the proposed method's robustness to variables of disparity, a thorough sensitivity analysis was conducted using a data set consisting of synthetically generated images of targets provided by the NSWC - Panama City Division.

The characterizing difference among the method presented in this work and that of [1] are the statistics used to form detection decisions on whether or not an unknown but common signal is present within the data collected by a number of sensing systems. While the method presented in [1] forms the inner product of each pair-wise combination of channels to measure the overall coherence, the method of this work first projects the multi-channel data into a new coordinate system where the relations (linear) among the channels are maximized. The optimal Gauss-Gauss detector [7]- [8] for binary hypothesis testing in the composite multi-channel domain is then developed by deriving expressions for the log-likelihood ratio and J-divergence, a global measure of the amount of discriminatory information available for detection. However, one advantage of the statistic presented in [1] is the fact that the measure is nonparametric in the sense that no *a priori* information of the problem is needed before-hand.

This paper is organized as follows: Section II will review the MCA framework. Section III develops the MCA-based Gauss-Gauss detection method [7]- [8]. Section IV provides the results and discussion of the sensitivity analyses and finally concluding remarks will be made in Section V.

II. Multi-Channel Coherence Analysis

Consider N zero mean random vectors, $\mathbf{x}_1$, $\mathbf{x}_2$,..., and $\mathbf{x}_N$, representing multiple data channels comprising the composite data channel $\mathbf{z} = \left[\mathbf{x}_1^H \ \mathbf{x}_2^H \ \cdots \ \mathbf{x}_N^H\right]^H \in \mathbb{C}^{d\times 1}$. Without loss of generality, we will assume all random vectors to be zero mean throughout this analysis. Let each channel $\mathbf{x}_j \in \mathbb{C}^{d_j\times 1}$ be of dimension d_j, where it is assumed that $\mathbf{x}_1$ is of the smallest dimension and we denote $d = \sum_{j=1}^{N} d_j$. The $d \times d$ dimensional covariance matrix of the composite data channel $\mathbf{z}$ is given by

$$R_{\mathbf{zz}} = E\left[\mathbf{z}\mathbf{z}^H\right] = \begin{bmatrix} R_{11} & R_{12} & \cdots & R_{1N} \\ R_{21} & R_{22} & \cdots & R_{2N} \\ \vdots & \vdots & \ddots & \vdots \\ R_{N1} & R_{N2} & \cdots & R_{NN} \end{bmatrix}, \quad (1)$$

where $R_{jk} = E[\mathbf{x}_j\mathbf{x}_k^H]$ is the auto-covariance ($j = k$) or cross-covariance ($j \neq k$) matrices of data channels $\mathbf{x}_j$ and $\mathbf{x}_k$ and clearly we have $R_{jk} = R_{kj}^H$.

Similar to Canonical Correlation Analysis (CCA) [9], [10] the i^{th} multi-channel coordinate of the j^{th} channel is found by searching for the i^{th} coordinate mapping vector, $\boldsymbol{\alpha}_{i,j}$, of data channel $\mathbf{x}_j$. This linear transformation produces the i^{th} multi-channel coordinate for the j^{th} channel,

$$v_{ij} = \boldsymbol{\alpha}_{i,j}^H \mathbf{x}_j. \quad (2)$$

If the i^{th} coordinate mapping vectors are found for all N channels, we can then obtain the *composite coordinate mapping* vector $\mathbf{a}_i = \left[\boldsymbol{\alpha}_{i,1}^H \ \boldsymbol{\alpha}_{i,2}^H \ \cdots \ \boldsymbol{\alpha}_{i,N}^H\right]^H$ which is then used to find the *composite coordinate* vector $\mathbf{v}_i = [v_{i,1} \ v_{i,2} \ \cdots \ v_{i,N}]^T = \left[\mathbf{x}_1^H\boldsymbol{\alpha}_{i,1} \ \mathbf{x}_2^H\boldsymbol{\alpha}_{i,2} \ \cdots \ \mathbf{x}_N^H\boldsymbol{\alpha}_{i,N}\right]^H$ which consists of the i^{th} multi-channel coordinate of every channel. The associated covariance matrix of $\mathbf{v}_i$ is given by

$$\begin{aligned} R_{\mathbf{v}_i\mathbf{v}_i} &= E\left[\mathbf{v}_i\mathbf{v}_i^H\right] \\ &= \begin{bmatrix} \boldsymbol{\alpha}_{i,1}^H R_{11}\boldsymbol{\alpha}_{i,1} & \cdots & \boldsymbol{\alpha}_{i,1}^H R_{1N}\boldsymbol{\alpha}_{i,N} \\ \vdots & \ddots & \vdots \\ \boldsymbol{\alpha}_{i,N}^H R_{N1}\boldsymbol{\alpha}_{i,1} & \cdots & \boldsymbol{\alpha}_{i,N}^H R_{NN}\boldsymbol{\alpha}_{i,N} \end{bmatrix} \end{aligned} \quad (3)$$

Recall that in the two-channel CCA [7], [11], the correlations between the mapped coordinates are maximized subject to the constraint that the transformed coordinates have unit variance. In the multi-channel case, however, the analysis is not as well-defined as all correlations between all possible pairs of channels must be maximized simultaneously. To accomplish this, one approach that has been proposed [6] is to maximize the sum of all correlations (the SUMCOR objective function) subject to the unit trace constraint of matrix $R_{\mathbf{v}_i\mathbf{v}_i}$. Thus, the optimization problem for finding the first composite coordinate mapping vector $\mathbf{a}_1$ using the objective function and constraint just described becomes

$$\begin{aligned} \mathbf{a}_1 &= \arg\max_{\mathbf{a}_1} \sum_{j=1}^{N}\sum_{k=1}^{N} \boldsymbol{\alpha}_{1,j}^H R_{j,k}\boldsymbol{\alpha}_{1,k} \\ &= \arg\max_{\mathbf{a}_1} \sum_{j=1}^{N}\sum_{k=1}^{N} \left[R_{\mathbf{v}_1\mathbf{v}_1}\right]_{j,k} \end{aligned} \quad (4)$$

subject to the constraint

$$\mathrm{tr}\left(R_{\mathbf{v}_1\mathbf{v}_1}\right) = \sum_{j=1}^{N} \boldsymbol{\alpha}_{1,j}^H R_{jj}\boldsymbol{\alpha}_{1,j} = 1,$$

It is shown [6] that the constrained optimization problem for the first coordinate mapping vectors, $\boldsymbol{\alpha}_{1,j}$ using a Lagrange multiplier method leads to

$$\sum_{k=1}^{N} R_{jk}\boldsymbol{\alpha}_{1,k} = \lambda_1 R_{jj}\boldsymbol{\alpha}_{1,j}, \quad \forall \ \ j,k \in [1,N]$$

or in matrix notation as

$$R_{\mathbf{zz}}\mathbf{a}_1 = \lambda_1 D\mathbf{a}_1, \quad (5)$$

where D is a block diagonal matrix with diagonal blocks $R_{jj}, \ \forall \ j \in [1, N]$, i.e.

$$D = \text{diag}\left[R_{11}, R_{22}, \ldots, R_{NN}\right]. \tag{6}$$

The result in (5) represents a generalized eigenvalue problem for which standard methods of solution are well-known. We will then consider the simultaneous solution to all mapping vectors $\mathbf{a}_i$'s, $i \in [1, d]$ and write (5) as $R_{\mathbf{zz}}A = DA\Lambda$ where A consists of all d coordinate mapping vectors, and Λ consists of all d eigenvalues. This solution can then be rewritten in terms of a standard eigenvalue problem $EP = P\Lambda$ where $E = D^{-\frac{1}{2}}R_{\mathbf{zz}}D^{-\frac{H}{2}}$ and P is a unitary matrix $\left(PP^H = P^HP = I\right)$. Clearly, we can find the mapping matrix A via $A = D^{-\frac{H}{2}}P$. Inspection of matrix E shows that it is simply the composite covariance matrix of the whitened version of $\mathbf{z} = \left[\ \mathbf{x}_1^H \ \cdots \ \mathbf{x}_N^H\ \right]^H$. That is, if we define this whitened version of the composite data channel vector by $\mathbf{w} = \left[\ \mathbf{w}_1^H \ \cdots \ \mathbf{w}_N^H\ \right]^H = D^{-\frac{1}{2}}\mathbf{z}$, then the whitened composite vector $\mathbf{w}$ has correlation matrix $E\left[\mathbf{w}\mathbf{w}^H\right] = D^{-\frac{1}{2}}R_{\mathbf{zz}}D^{-\frac{H}{2}} = E$. Matrix P is then used to map the whitened channels to their multi-channel coordinates. In order to find mapping vectors corresponding to the principal coordinates [6], we only consider the $r = d_1 = \min_j\{d_j\}$ coordinates such that $\lambda_1 > \lambda_2 > \ldots > \lambda_r$. Thus, $\Lambda = \text{diag}\left[\lambda_1, \lambda_2, \ldots, \lambda_r\right]$ will become a $r \times r$ diagonal matrix composed of the dominant eigenvalues and P will become a $d \times r$ matrix composed of the eigenvectors corresponding to r dominant eigenvalues. To find the mapped coordinate vector, $\mathbf{v}$, that contains all mapped coordinates for all N channels, we will first define Ψ_j (dimension $d_j \times r$) to contain those dominant r eigenvectors $\mathbf{p}_{i,j}, \ \forall \ i \in [1, r]$ of the mapping matrix P that correspond to the j^{th} channel

$$\Psi_j = \left[\ \mathbf{p}_{1,j} \quad \mathbf{p}_{2,j} \quad \cdots \quad \mathbf{p}_{r,j}\ \right], \ \forall\, j \in [1, N]. \tag{7}$$

Clearly, the connection between P and Ψ_j is evident

$$P = \begin{bmatrix} \Psi_1 \\ \Psi_2 \\ \vdots \\ \Psi_N \end{bmatrix}_{d \times r}. \tag{8}$$

Note that in the case of two channels, Ψ_1 and Ψ_2 are directly related to the mapping matrices of CCA [8]. All of the mapped coordinates of the j^{th} channel can then be found by

$$\boldsymbol{\mu}_j = \Psi_j^H R_{jj}^{-\frac{1}{2}}\mathbf{x}_j, \quad \forall \ \ j \in [1, N], \tag{9}$$

where $\boldsymbol{\mu}_j = \left[\ v_{1,j} \quad v_{2,j} \quad \cdots \quad v_{r,j}\ \right]^T$. Clearly, we have the following two properties

$$\begin{aligned} \sum_{j=1}^{N} E\left[\boldsymbol{\mu}_j\boldsymbol{\mu}_j^H\right] &= \sum_{j=1}^{N} \Psi_j^H\Psi_j = I \\ \sum_{j=1}^{N}\sum_{k=1}^{N} E\left[\boldsymbol{\mu}_j\boldsymbol{\mu}_k^H\right] &= \sum_{j=1}^{N}\sum_{k=1}^{N} \Psi_j^H R_{jj}^{-\frac{1}{2}} R_{jk} R_{kk}^{-\frac{H}{2}} \Psi_k = \Lambda \end{aligned}$$

If we define block diagonal matrix $\boldsymbol{\Psi}$ that contains the Ψ_j matrices along its diagonal blocks, i.e. $\boldsymbol{\Psi} = \text{diag}\left[\Psi_1, \Psi_2, \ldots, \Psi_N\right]$, then we can resolve all N channels into their multi-channel coordinates using

$$\mathbf{v} = \boldsymbol{\Psi}^H\mathbf{w} = \boldsymbol{\Psi}^H D^{-\frac{1}{2}}\mathbf{z}. \tag{10}$$

III. MCA Detection

A classical detection problem is that of choosing between two hypotheses that are relevant to the given problem. For this coherence-based detector, the null hypothesis (H_0) is the hypothesis that all N channels consist of background noise and the alternative hypothesis (H_1) that all N channels consist of signal plus noise. Figure 1 shows the graphical setup of the problem under consideration. Several simplifying but sensible assumptions used in this analysis are

1) Noise between different channels is mutually uncorrelated, i.e. $E\left[\mathbf{n}_j\mathbf{n}_k^H\right] = 0 \ \forall \ j, k \in [1, N], \ j \neq k$.
2) Signal is uncorrelated with the background noise, i.e. $E\left[\mathbf{s}_j\mathbf{n}_k^H\right] = E\left[\mathbf{n}_j\mathbf{s}_k^H\right] = 0 \ \forall \ j, k \in [1, N]$.
3) Noise contained on any one channel has covariance matrix, i.e. $E\left[\mathbf{n}_j\mathbf{n}_j^H\right] = R_{\mathbf{n}_j} \ \forall \ j \in [1, N]$.
4) Signal contained on any pair of channels has covariance matrix, i.e. $E\left[\mathbf{s}_j\mathbf{s}_k^H\right] = R_{\mathbf{s}_{jk}} \ \forall \ j, k \in [1, N]$.

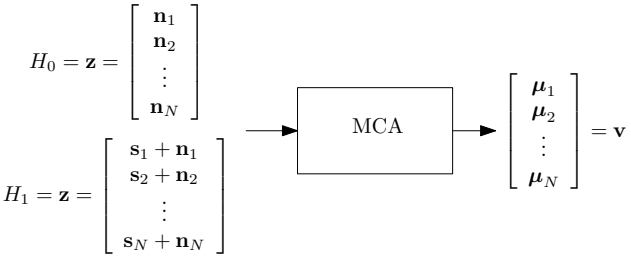

Fig. 1. Multi-Channel Hypothesis Test and MCA.

Under H_0, the matrices $R_{\mathbf{zz}}$ and D become

$$R_{\mathbf{zz}_0} = D_0 = \text{diag}\left[R_{\mathbf{n}_1}, R_{\mathbf{n}_2}, \ldots, R_{\mathbf{n}_N}\right].$$

Note that the subscript notation refers to the hypothesis being considered. Thus, the solution to the eigenvalue problem under H_0 leads to $\Lambda_0 = I$, while for A_0 no unique solution exists. Now, since any non-zero vector will satisfy the generalized eigenvalue problem, for simplicity we choose the eigenvectors of the null hypothesis to be the same as those of the alternative hypothesis, i.e. $A_0 = A_1 = A$.

Under H_1 and using the stated assumptions, the corresponding $R_{\mathbf{zz}}$ and D matrices are

$$R_{\mathbf{zz}_1} = \begin{bmatrix} R_{\mathbf{s}_{11}} + R_{\mathbf{n}_1} & R_{\mathbf{s}_{12}} & \cdots & R_{\mathbf{s}_{1N}} \\ R_{\mathbf{s}_{21}} & R_{\mathbf{s}_{22}} + R_{\mathbf{n}_2} & \cdots & R_{\mathbf{s}_{2N}} \\ \vdots & \vdots & \ddots & \vdots \\ R_{\mathbf{s}_{N1}} & R_{\mathbf{s}_{N2}} & \cdots & R_{\mathbf{s}_{NN}} + R_{\mathbf{n}_N} \end{bmatrix}$$

$$D_1 = \text{diag}\left[R_{\mathbf{s}_{11}} + R_{\mathbf{n}_1}, R_{\mathbf{s}_{22}} + R_{\mathbf{n}_2}, \ldots, R_{\mathbf{s}_{NN}} + R_{\mathbf{n}_N}\right]$$

leading to the following arbitrary eigenvalue problem.

$$R_{\mathbf{zz}_1}A_1 = D_1A_1\Lambda_1 \tag{11}$$

The log-likelihood ratio that minimizes the risk involved in deciding between the two hypotheses is defined [12] to be

$$l(\mathbf{z}) = \ln\left[\frac{p(\mathbf{z}|H_1)}{p(\mathbf{z}|H_0)}\right] \tag{12}$$

which is compared to a global threshold η to form the discriminant function $\gamma(\mathbf{z})$,

$$\gamma(\mathbf{z}) = \begin{cases} 1 \sim H_1 & l(\mathbf{z}) \geq \eta \\ 0 \sim H_0 & l(\mathbf{z}) < \eta \end{cases}$$

Assuming that under both hypotheses the composite data channel $\mathbf{z}$ is multivariate Gaussian with zero mean and covariance matrix $R_{\mathbf{zz}}$, the log-likelihood ratio of the composite data vector becomes

$$l(\mathbf{z}) = \mathbf{z}^H \left(R_{\mathbf{zz}_0}^{-1} - R_{\mathbf{zz}_1}^{-1}\right) \mathbf{z}. \tag{13}$$

Next, we can formulate $R_{\mathbf{zz}}^{-1}$ in terms of the sum of the correlations of each coordinate and their corresponding eigenvectors. To do this, we recall the fact that $P^H E P = \Lambda$. Taking the inverse of this relationship, it is simple to show that $R_{\mathbf{zz}}^{-1} = A\Lambda^{-1}A^H$. Thus, the log-likelihood function in (13) becomes

$$l(\mathbf{z}) = \mathbf{z}^H \left(A_0\Lambda_0^{-1}A_0^H - A_1\Lambda_1^{-1}A_1^H\right) \mathbf{z}.$$

Since the eigenvalues under the null hypothesis are all one, i.e. $\Lambda_0 = I$, and owing to the lack of a unique solution for the mapping matrices of the null hypothesis, we can write the log-likelihood ratio as

$$l(\mathbf{z}) = \mathbf{z}^H \left[A_1 \left(I - \Lambda_1^{-1}\right) A_1^H\right] \mathbf{z}, \tag{14}$$

where A_1 and Λ_1 are the mapping matrix and diagonal matrix of multi-channel correlations, respectively, for the set of data with which we are performing the hypothesis test.

Next, we will formulate the J-divergence [11], [13] which is a measure of the separability of the two hypotheses. The J-divergence is defined to be

$$J = E_{H_1}\left[l(\mathbf{z})\right] - E_{H_0}\left[l(\mathbf{z})\right], \tag{15}$$

where $E_{H_1}[\,\cdot\,]$ and $E_{H_0}[\,\cdot\,]$ represent the expectation operation evaluated under the H_1 and H_0 hypotheses, respectively. The expected value of the log-likelihood function becomes

$$E\left[l(\mathbf{z})\right] = E\left[tr\left(\mathbf{z}^H Q \mathbf{z}\right)\right]. \tag{16}$$

Where $Q = \left(R_{\mathbf{zz}_0}^{-1} - R_{\mathbf{zz}_1}^{-1}\right)$. Using the cyclic property of the trace, we can write

$$\begin{aligned} E\left[l(\mathbf{z})\right] &= E\left[tr\left(Q\mathbf{z}\mathbf{z}^H\right)\right] \\ &= tr\left(QR_{\mathbf{zz}}\right). \end{aligned} \tag{17}$$

Thus, we can write the J-divergence as

$$\begin{aligned} J &= E_{H_1}\left[l(\mathbf{z})\right] - E_{H_0}\left[l(\mathbf{z})\right] \\ &= tr\left(QR_{\mathbf{zz}_1}\right) - tr\left(QR_{\mathbf{zz}_0}\right) \\ &= tr\left[-2I + R_{\mathbf{zz}_0}^{-1}R_{\mathbf{zz}_1} + R_{\mathbf{zz}_1}^{-1}R_{\mathbf{zz}_0}\right]. \end{aligned} \tag{18}$$

Rearranging and using the cyclic property of the trace, we can write the J-divergence as

$$J = tr\left[-2I + \Lambda_1 + \Lambda_1^{-1}\right] = \sum_{i=1}^{r}\left(-2 + \lambda_i + \lambda_i^{-1}\right). \tag{19}$$

Therefore, the only pieces of information we need to know when performing detection in this framework are the matrices A_1 and Λ_1.

IV. Simulation Results

A. Data Description and Pre-Processing

This N-channel coherence-based detection method was then applied to a data set consisting of synthetically generated sonar images (snippets) of both targets and non-targets of different geometrical shapes. The sonar snippets were generated with different resolutions, SNR, range, and aspect angles mimicking different realistic operating conditions. For this study, two different resolutions, namely $1in$ and $3in$, were considered. Additionally, SNR ranged from $0dB$ to $15dB$ in increments of $3dB$, range values spanned from $10m$ to $120m$ in increments of $1m$, and aspect angle ranged anywhere from 0° to 360° in increments of 1°. A subset of the data corresponding to target snippets was used to represent the H_1 hypothesis while background snippets were used to represent the H_0 hypothesis. Thus, all non-target snippets were excluded. The subset of target snippets (1610 snippets) was further partitioned into 3 different parts forming 138 cone-type targets, 736 cylinder-type targets, and 736 trapezoidal-type targets. When performing detection, each of the N images is partitioned into blocks of size dependent on the resolution. Each block is then channelized and used to form a realization of the composite data vector, $\mathbf{z}$. The ensemble set formed from all realizations pertaining to that set of N images is then used to form the sample composite covariance matrix $R_{\mathbf{zz}}$ which is then decomposed by the MCA process and used to form the discriminant function, $l(\mathbf{z})$ in (14). Each block (realization) from the ensemble set is then applied to the log-likelihood ratio test and if 50% or more of the blocks pass, that set of N snippet images is said to contain a target. Figure 2 displays the process behind the MCA-based detection system used for this analysis.

B. Dual Resolution Disparate Detection Performance

In some disparate detection applications, each platform may carry multiple sensing systems with different spatial and spectral characteristics in order to highlight different attributes of the target. To simulate such a situation, a two-channel detection problem was constructed where each channel consisted of snippets of targets of the same type at the same range, aspect angle, and SNR. However, the two channels differed in resolution, one snippet-image of high resolution ($1in$) and the other of a lower resolution ($3in$). When performing detection, a 4×4 block size was used for the high resolution images and a 2×1 block size for those of lower resolution. This setup was then run for all 1610 images at various ranges and aspect

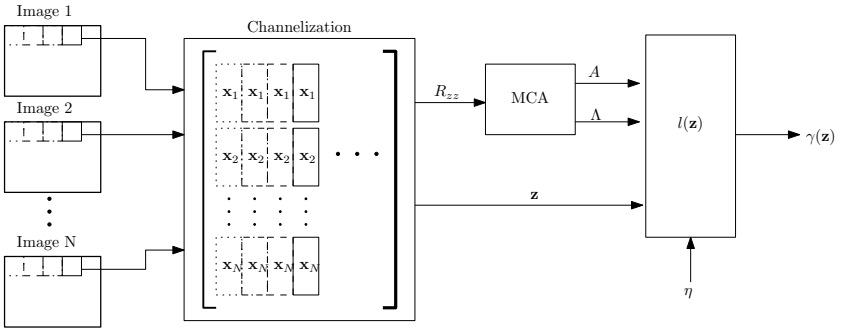

Fig. 2. N-Channel MCA Detector.

angles and the results partitioned on the basis of target type and SNR.

Figures 3(a)-(c) display the ROC curves for conical, cylindrical, and trapezoidal type targets, respectively, at three different SNR values of $0dB$, $6dB$, and $12dB$, respectively. Figures 4(a)-(c), on the other hand, display sensitivity to target types for a given SNR. Table I gives the probability of detection at the knee point of the ROC, i.e. where $P_d + P_{fa} = 1$, for all target types and SNR values. As can be observed from the results in Table I, it is apparent that for cylindrical and trapezoidal targets the detection performance generally improves as a function of SNR as one would expect. However, the performance of the detector for the cone targets does not follow the same behavior. This may be attributed, in part, to the fact that only a small number of cone targets were available for this study.

TABLE I
PROBABILITY OF DETECTION (%) VS. SNR

Target Type	$0dB$	$3dB$	$6dB$	$9dB$	$12dB$	$15dB$
Cone	91.30	94.93	96.38	89.86	81.16	87.68
Cylinder	83.70	85.19	82.20	85.33	89.67	94.02
Trapezoid	84.24	84.51	84.65	85.73	90.08	93.75

C. Dual Aspect Angle Separation Disparate Detection Performance

Another question that may arise in any disparate detection problem is that of sensor locations. That is, for different types of targets how does the detection performance change as a function of disparities in location of the sensor platforms. This clearly relates to the target's aspect/orientation with respect to the sensor platform as well as the range of the platform from the target. To determine the answer to this question, a study is carried out where both channels consisted of images of the same resolution ($1in$), at ranges within $\pm 1m$ of one another, and at an identical SNR of $9dB$, while the disparateness was with respect to aspect angle separation. More specifically, the two channels correspond to sonar snippet-images from the same target at two aspect angles with separation angle θ such that if ϕ_1 and ϕ_2 represent the aspect angles associated with their respective image then pairs of images were chosen such that $|\phi_1 - \phi_2| \in [\theta - \delta, \theta + \delta]$, where δ represents the perturbation from the separation angle, θ, due to non-uniform motion of the vehicle. Here, the value of δ was chosen to be 10°. The aspect angle separation θ was then varied from 0° to 180° in increments of 30° and its affect on the performance of the detector was studied. Figures 5(a) and (b) display the ROC curves for cylindrical and trapezoidal targets, respectively, for several values of θ. Note that all images in the database corresponding to cone targets were generated at an angle of 0° and thus excluded from this study. Table II gives the probability of detection at the knee point of the ROC versus aspect angle separation and target type. From both Figures 5(a) and (b) and the results in Table II, it can be concluded that the performance of the detector is fairly robust to disparateness in aspect angle separation as the probability of detection at the knee point of the ROC never falls below 92%.

TABLE II
PROBABILITY OF DETECTION (%) VS. ASPECT ANGLE SEPARATION (θ)

Target Type	0°	30°	60°	90°	120°	150°	180°
Cylinder	94.40	96.14	97.83	98.33	97.47	96.82	94.92
Trapezoid	92.86	96.29	97.21	97.66	97.57	96.09	93.14

Figure 6 displays the plots of empirical J-divergence as a function of aspect angle separation, θ, for both cylindrical and trapezoidal targets. Both curves were generated by empirically estimating the difference in means of the log-likelihood ratio among target (H_1) and noise (H_0) snippets and averaging over all such pairs of images that match the criteria explained previously (i.e. same SNR, same resolution, ranges within $1m$, aspect separation within some range of a particular angle). The results in Figure 6 match what was observed in Figures 5(a) and (b) as the performance of the detector seems to improve as the separation in aspect angle deviates from 0° and 180°. Again we can draw the same conclusion that the detector is fairly robust to separation in aspect angles as the difference between maximum and minimum J-divergence never grows larger than approximately 0.6. Additionally, the J-divergence values for cylindrical target are higher than those of trapezoidal target. This result is also evident in the ROC plots of Figures 5(a) and (b).

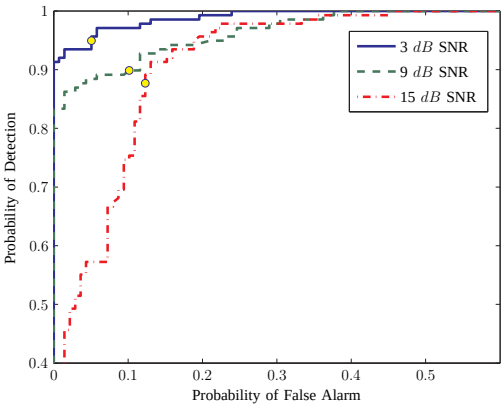

(a) Cone Target Type

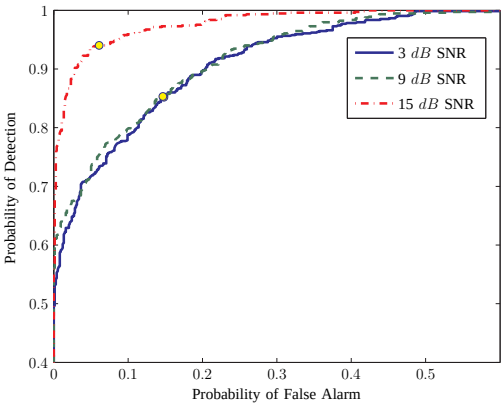

(b) Cylindrical Target Type

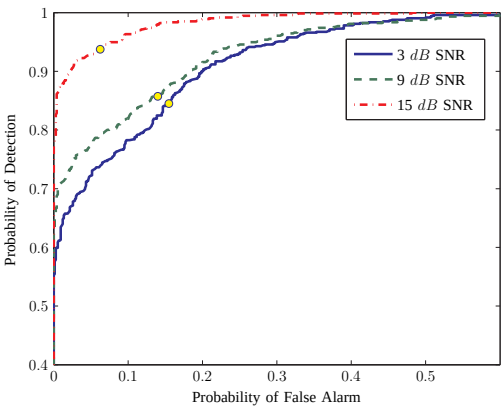

(c) Trapezoidal Target Type

Fig. 3. Detector Performance for Different Target Types vs. SNR.

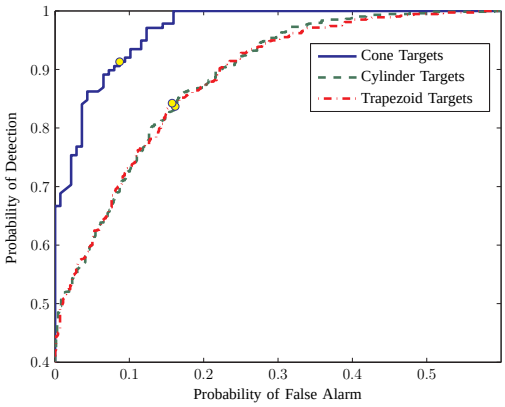

(a) $0dB$ SNR

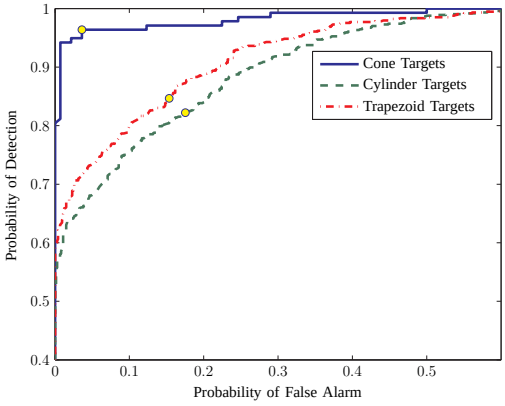

(b) $6dB$ SNR

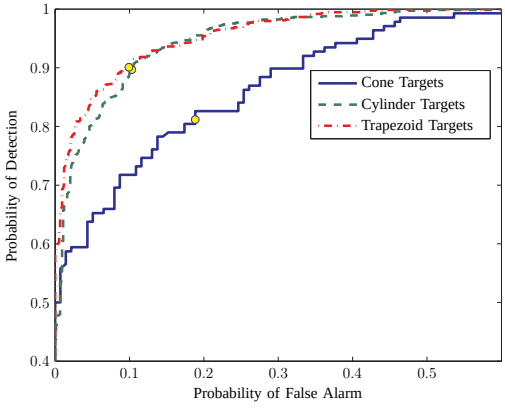

(c) $12dB$ SNR

Fig. 4. Detector Performance for Various SNR Values vs. Target Type.

V. Conclusion

In this paper, a multi-channel, multi-sensory binary hypothesis detection system has been introduced using the MCA framework. An N-channel Gauss-Gauss detector was then formulated in the MCA coordinates. Detection is performed by extracting the multi-channel mapping vectors and the correlation sums from the data samples collected by the sensory platforms. These mapping vectors and coherent features are then used in the log-likelihood ratio to detect targets in the sonar images. This MCA-based detector is then applied to a synthetic sonar image data set to investigate the performance of the detector to different sensing disparities. These studies

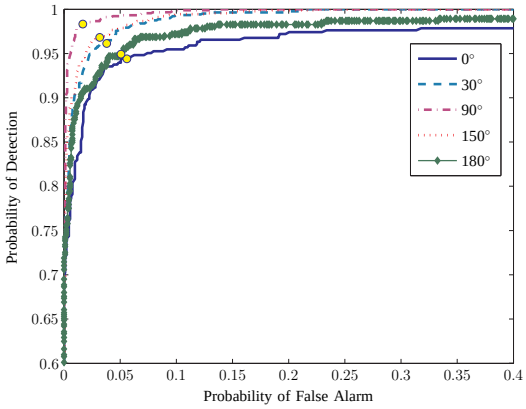

(a) Cylindrical Target Type

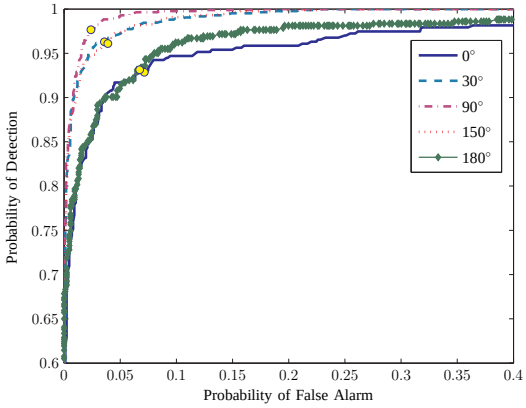

(b) Trapezoidal Target Type

Fig. 5. Detector Performance for Two Target Types vs. Aspect Angle Separation.

were specifically focused on the dual channel detection problem as the data set did not allow for more than 2 channels. We evaluated the detector performance versus differences in target types, SNRs, and aspect angles. The detector was found to be robust to SNR changes across most of the target types and robust to varying degrees of aspect separation by observing the probability of detection at the knee point of the ROC curve. Furthermore, the J-divergence was empirically estimated and shown to also be robust to disparities in aspect angle separation. Through this work we have shown that MCA provides an elegant framework when performing coherence-based detection among multiple disparate sensory channels.

ACKNOWLEDGMENT

This work was supported by the Office of Naval Research, Code 321OE under contract #N00014-08-1-0142.

REFERENCES

[1] D. Cochran, H. Gish, and D. Sinno, "A geometric approach to multiple-channel signal detection," *IEEE Transactions on Signal Processing*, vol. 43, pp. 2049–2057, September 1995.

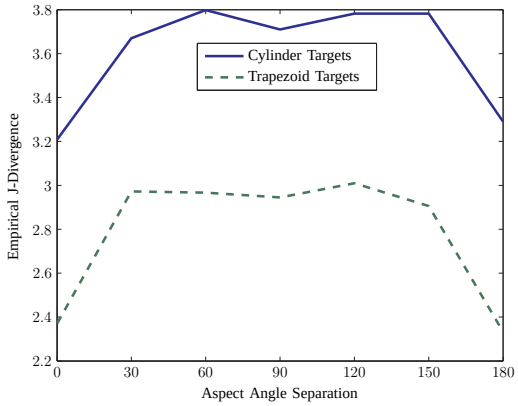

Fig. 6. J-Divergence vs. Aspect Angle Separation.

[2] G. J. Dobeck, J. Hyland, and L. Smedley, "Automated detection/classification of sea mines in sonar imagery," *Proc. SPIE*, vol. 3079, pp. 90–110, April 1997.

[3] T. Aridgides, P. Libera, M. Fernandez, and G. J. Dobeck, "Adaptive filter/feature orthogonalization processing string for optimal LLRT mine classification in side-scan sonar imagery," *Proc. SPIE*, vol. 2765, pp. 110–121, April 1996.

[4] T. Aridgides and M. Fernandez, "Enhanced ATR algorithm for high resolution multi-band sonar imagery," *Proc. SPIE*, vol. 6953, pp. 0H1–0H10, March 2008.

[5] N. Klausner, M. R. Azimi-Sadjadi, and J. D. Tucker, "Underwater target detection from multi-platform sonar imagery using multi-channel coherence analysis," *Proc. of SMC 2009 Conference*, to be published.

[6] B. Thompson and M. Azimi-Sadjadi, "Iterative multi-channel coherence analysis with applications," *Neural Networks*, vol. 21, pp. 493–501, 2008.

[7] A. Pezeshki, L. Scharf, J. Thomas, and B. Van Veen, "Canonical coordinates are the right coordinates for low-rank Gauss-Gauss detection and estimation," *IEEE Transactions on Signal Processing*, vol. 54, pp. 4817–4820, December 2006.

[8] L. Scharf and C. Mullis, "Canonical coordinates and the geometry of inference, rate, and capacity," *IEEE Transactions on Signal Processing*, vol. 48, pp. 824–831, March 2000.

[9] H. Hotelling, "Relations between two sets of variates," *Biometrika*, vol. 28, pp. 321–377, 1936.

[10] A. Rencher, *Methods of Multivariate Analysis*, 2nd ed. Wiley-Interscience, 2002.

[11] L. Scharf and B. Van Veen, "Low rank detectors for Gaussian random vectors," *IEEE Transactions on Acoustics, Speech, and Signal Processing*, vol. 35, pp. 1579–1582, November 1987.

[12] H. L. Van Trees, *Detection, Estimation, and Modulation Theory Part I*. John Wiley and Sons, 1968.

[13] S. Kullaback, *Information Theory and Statistics*. New York: Dover, 1968.